Published in "Inorganic Chemistry 58(20): 13796–13806, 2019"
which should be cited to refer to this work.

Sequential Multiple-Target Sensor: In^{3+}, Fe^{2+}, and Fe^{3+} Discrimination by an Anthracene-Based Probe

Alba Finelli,[†] Valentin Chabert,[†] Nelly Hérault,[†] Aurélien Crochet,[‡] Cheal Kim,[§] and Katharina M. Fromm*[,†]

[†]Department of Chemistry, University of Fribourg, Ch. du Musée 9, 1700 Fribourg, Switzerland

[‡]FriMat, Department of Chemistry, University of Fribourg, Ch. du Musée 9, 1700 Fribourg, Switzerland

[§]Department of Fine Chemistry, Seoul National University of Science and Technology (SeoulTech), Seoul 139-743, Republic of Korea

Supporting Information

ABSTRACT: Indium is a nonphysiological toxic metal widely used in industry. While misunderstood, its toxicity is proposed to be linked to a perturbation of Fe^{3+} homeostasis through the binding of In^{3+} ions to essential iron metalloproteins such as transferrins. Therefore, the monitoring of In^{3+} and Fe^{3+} in biological environments is of prime interest for both basic research and diagnosis. Here we report the design of a salen-type anthracene-based probe able to selectively sense and discriminate In^{3+} and $Fe^{2+/3+}$ ions by fluoro-colorimetry.

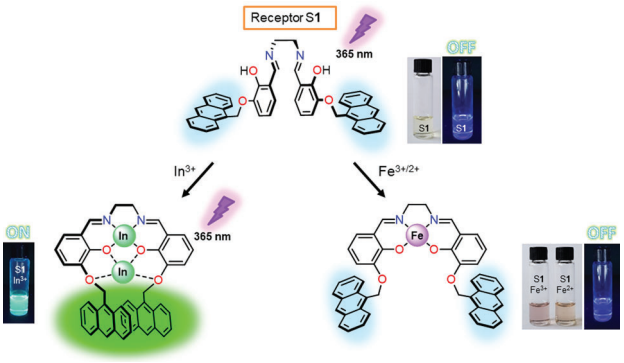

INTRODUCTION

Physiological metal ions play key roles in all kingdoms of life, and their homeostasis is finely regulated. Being the most abundant transition metal on earth, iron is involved in many biological processes such as DNA synthesis, oxygen transport, or electron transfer. Hence, slight perturbations of its cellular homeostasis can lead to severe diseases, such as Parkinson or Alzheimer diseases.[1,2] On the other hand, the industrial use of metals leads to a release of nonphysiological metal ions into the environment, increasing their bioavailability and hence the frequency of associated diseases. Nowadays, the industrial use of indium is globally increasing due to the growth of photovoltaic and optoelectronic industries[3−5] with the global indium market estimated at 810 tons in 2016.[6] While toxicity and exposure data are limited for this metal,[7−9] recent reports highlighted the involvement of indium in lung diseases of exposed workers.[10−15] Indeed, indium has been proposed to perturb alveolar macrophage functions, resulting in the so-called indium lung disease.[16] Furthermore, the biochemical similarities between In^{3+} and Fe^{3+} ions (ionic radii of 94 pm and 78.5 pm (high spin)/69 pm (low spin), in octahedral environment, respectively)[17] may be responsible for a disruption of the iron metabolism by indium, resulting in imbalances at iron absorption sites, transportation, usage, and storage in cells.[18] For instance, the iron transport has been proposed to be inhibited by indium ions, due to their tight binding to transferrins.[19] Indeed, possessing the same charge, In^{3+} ions can accommodate in Fe^{3+} binding sites of transferrins with a high affinity. For Fe^{3+} detection, numerous probes have been recently reported.[20−22] For instance, Lee et al. have reported a selective rhodamine-based sensor showing a sensitive and selective detection of intracellular Fe^{3+} ions in hepatocytes.[23,24] To the best of our knowledge, Kim and co-workers were the first in synthesizing an indium sensor, based on pyrene moieties.[25] Due to the high interest of monitoring In^{3+} concentrations in biological environments, the number of optical probes for In^{3+} detection is also increasing.[26−35] Nevertheless, the design of new chemosensors able to quantify the cellular concentrations of iron and indium ions is still needed for the fundamental understanding of indium toxicity as well as for the diagnosis of associated diseases.

Lately, considerable efforts have been made in the conception of new chemosensors for the selective detection of multiple metal ions.[36−42] Among the available sensing methods, probes based on metal ion-induced fluorescence changes are principally attractive and offer many advantages such as the selectivity, the fast responses, and the high sensitivity.[43−45] However, due to the fluorescence quenching effects by certain metal ions,[46] the development of turn-on fluorescence chemosensors remains very challenging. On the other hand, the colorimetric method represents an easy and fast technique allowing detection of targets by a color change, ideally even visible with the naked-eye.[47−50]

In order to design a versatile probe especially able to discriminate In^{3+} among other cations, Schiff base ligands have caught our attention.[51−56] Azomethine ligands, such as salen and its derivatives, which are commonly used as chelating ligands in coordination chemistry, are of crucial interest in multiple areas such as supramolecular chemistry,[57,58] material sciences,[59−61] or catalysis.[62−64] Furthermore, salen based ligands are well-known to coordinate In^{3+} cations with their N_2O_2 chelating site, producing complexes which are widely used as efficient catalysts for e.g. isoselective lactide polymerization.[65,66] Such compounds are easy to prepare and are readily tunable.

Building on this framework, we developed the first fluorescent and colorimetric multitarget anthracene-based sensor **S1** able to distinguish indium and iron through distinct optical methods. This multisensing probe is able to selectively detect In^{3+} ions with a strong excimer fluorescence emission and selectively senses Fe^{2+}/Fe^{3+} ions by the formation of a broad charge transfer (CT) band involving the inner O_2O_2 and outer N_2O_2 coordination spheres of **S1** and giving rise to a red color of the complex.

EXPERIMENTAL SECTION

Materials and Methods. All experiments were performed in air and at RT. Ligand **S1** was prepared based on the procedure reported previously by Mandolini and co-workers.[67] All chemicals were commercial products of reagent grade and were used without further purification. ^1H and ^{13}C NMR measurements were carried out with a Bruker 400 MHz spectrometer at ambient temperature, and chemical shifts are given in ppm with respect to the residual solvent peak. Mass spectra (ESI-TOF, positive mode) were recorded with a Bruker esquire HCT spectrometer with a DMF/ACN mixture as solvent. The UV-vis spectra were recorded with a Perkin−Elmer Lambda 40 spectrometer. The spectrofluorimetric studies have been conducted on a Varian Cary Eclipse spectrofluorimeter.

Sensor Synthesis. *Synthesis of Anthracene-Based Aldehyde **S1′**.* To a suspension of pure NaH (0.73 mg, 2.8 equiv) in dry DMSO (3 mL) was added a solution of 2, 3-dihydroxybenzaldehyde (152 mg, 1.1 mmol) in DMSO (2 mL) at 20−25 °C. After stirring for 90 min, a solution of 9-bromomethylanthracene (300 mg, 1.1 mmol) in DMSO (2 mL) was added. Stirring was continued for 20−24 h in the dark, whereupon the mixture was poured into water (25 mL) and extracted with $CHCl_3$ (3 × 20 mL). The aqueous layer was acidified with 6 M HCl to adjust the pH to 4 and again extracted with $CHCl_3$ (3 × 50 mL). The combined $CHCl_3$ layers were washed with 1 M HCl (2 × 20 mL). The solvent was evaporated, and the residue was purified by column chromatography (silica gel, DCM/hexane (8:2)) to give the pure aldehyde **S1′** as a yellow solid (187.8 mg, 52%) (Figure S1). ^1H NMR (400 MHz, DMSO-d_6): δ 6.10 (s, 2H), 6.93−6.99 (t, J = 8 Hz, 1H), 7.27−7.30 (d, J = 4 Hz, 1H), 7.36−7.39 (d, J = 12 Hz, 1H), 7.46−7.58 (m, 4H), 8.02−8.05 (d, J = 8 Hz, 2H), 8.39−8.49 (d, J = 12 Hz, 2H), 8.52 (s, 1H), 9.93 (s, 1H), 11.04 (s, 1H). ^{13}C NMR (100 MHz, DMSO-d_6): δ 193.81, 151.61, 148.28, 131.45, 131.20, 129.37, 129.24, 127.54, 127.14, 125.75, 124.79, 123.00, 122.35, 122.08, 120.62, 120.32, 119,83, 64.01. ESI-mass: m/z calculated for $C_{22}H_{16}O_3$+Na^+ ($[M + Na]^+$), 351.09; found, 351.09.

*Synthesis of the Anthracene-Based Receptor **S1**.* The suspension of the corresponding aldehyde **S1′** (0.2 g, 0. 609 mmol, 2 equiv) was solubilized in MeOH (10 mL), and ethylenediamine was added slowly (0.0203 mL, 0.304 mmol). After letting the reaction stir at reflux overnight in the dark, the light-yellow product **S1** was collected by filtration and dried under vacuum (163.7 mg, 79%) (Figure S2). ^1H NMR (400 MHz, DMSO-d_6): δ 3.97 (s, 4H), 6.07 (s, 4H), 6.76−6.81 (t, J = 8 Hz, 2H), 6.93−6.96 (d, J = 8 Hz, 2H), 7.17−7.20 (d, J = 12 Hz, 2H), 7.54−7.44 (m, 8H), 8.00−8.03 (d, J = 12 Hz, 4H), 8.38 (s, 2H), 8.42−8.45 (d, J = 16 Hz, 4H), 8.50 (s, 2H), 13.67 (s, 2H). ^{13}C NMR (100 MHz, DMSO-d_6): δ 161.35, 157.60, 151.47, 150.09, 131.08, 129,31, 128.26, 126.58, 125.88, 125.70, 125.40, 124.40, 118.00, 115.94, 70.80, 67.7. ESI-mass: m/z calculated for $C_{46}H_{36}N_2O_4$+H^+ ($[M + H]^+$), 681.21; found, 681.27.

Sensing Tests of S1. Stock solutions (1 mM) of sensor **S1** (4.765 mg, 0.007 mmol) were prepared in DMF (7 mL). In order to obtain a solution with a final concentration of 40 μM, 24 μL of the previous solution (1 mM) was then diluted into 2.976 mL of DMF (3 mL in the cuvette). Metal ion salts were added from 0 to 3 equiv using 20 mM solutions of $M(NO_3)$ (M = Na, K, Ag), $M(NO_3)_2$ (M = Mn, Ni, Cu, Zn, Cd, Mg, Ca, Pb), $M(ClO_4)_2$ (M = Fe), and $M(NO_3)_3$ (M = Al, Fe, Cr, Ga, In) in DMF (addition of 9 μL, corresponding to 1.5 equiv), respectively. UV−vis and fluorescence spectra were recorded after mixing of the samples for a few seconds at ambient temperature.

*Fluorescence Titrations of **S1**.* For In^{3+}, a solution of 40 μM of sensor **S1** was prepared in a cuvette of 3 mL. Then, 6−90 μL of a solution of $In(NO_3)_3$ in DMF (5 mL, 20 mM) was added to the solutions of **S1** (40 μM) prepared previously. After mixing them for a few seconds, fluorescence spectra were recorded at 30 °C.

*UV−Vis Titrations of **S1**.* For Fe^{3+}, a solution of 40 μM of sensor **S1** was prepared in a cuvette of 3 mL. Then, 0.6−18 μL of a solution of $Fe(NO_3)_3$ in DMF (5 mL, 20 mM) was added to the solutions of **S1** (40 μM) prepared previously. After mixing them for a few seconds, UV−vis spectra were recorded at room temperature.

*NMR Titration of **S1**.* For In^{3+}, a solution of 0.5 mM in $CDCl_3$ of sensor **S1** was prepared in an NMR tube. Then, 1.7−10.2 μL of a solution of $In(NO_3)_3$ in MeOD (1.5 mM) was added to the solutions of **S1**. After mixing them for a few seconds, the ^1H NMR spectra were recorded at room temperature.

Job Plot Measurements. For In^{3+}, a stock solution (1 mM) of sensor **S1** (4.765 mg, 0.007 mmol) was prepared in DMF (7 mL). Volumes of 0, 18, 36, 54, 72, 90, 108, 126, 144, 162, and 180 μL of the chemosensor **S1** solutions (1 mM) were transferred to independent vials. In the same way, the volumes of 9, 8.1, 7.2, 6.3, 5.4, 4.5, 3.6, 2.7, 1.8, 0.9, and 0 μL of In^{3+} solutions (20 mM) were added to the correspondent diluted **S1** solution. Each vial is then filled with the latter solution to a total volume of 3 mL and after shaking them for a few seconds, fluorescence spectra were recorded at 30 °C.

For Fe^{2+} and Fe^{3+}, the same procedure has been adopted and the UV−vis spectra were recorded at room temperature.

Competition with Other Metal Ions. For Fe^{2+}/Fe^{3+} and In^{3+}, a stock solution (1 mM) of sensor **S1** (4.765 mg, 0.007 mmol) was prepared in DMF (7 mL). In order to obtain a solution with a final concentration of 40 μM, 24 μL of the previous solution (1 mM) was then diluted into 2.967 mL of DMF (3 mL in the cuvette). Metal ions salts were added (addition of 18 μL, corresponding to 3 equiv) using 20 mM solutions of $M(NO_3)$ (M = Na, K, Ag), $M(NO_3)_2$ (M = Mn, Ni, Cu, Zn, Cd, Mg, Ca, Pb), $M(ClO_4)_2$ (M = Fe), and $M(NO_3)_3$ (M = Al, Fe, Cr, Ga, In) in DMF, respectively. Then, 9 μL (corresponding to 3 equiv) of the analyzed metal ion, namely Fe^{2+}/Fe^{3+} and In^{3+} (40 mM solution), was added and the UV−vis or fluorescence spectra were recorded after mixing the samples for a few seconds at room temperature, respectively 30 °C.

RESULTS AND DISCUSSION

Ligand Synthesis and Characteristics. A salen-type compound has been modified via the introduction of two anthracene moieties, employed as chromophores for their efficient fluorogenic behavior. The anthracene derivative of the *o*-vanillin, **S1′**, was synthesized by a nucleophilic substitution reaction between 2,3-dihydroxybenzaldehyde and 9-bromomethylanthracene. The final anthracene ligand **S1** has been produced by a nucleophilic addition forming a hemiaminal, reacting ethylenediamine as starting material with the anthracene corresponding aldehyde **S1′**. The subsequent dehydration provides the resulting imine-based ligand **S1** (Scheme 1). The latter has been fully characterized by ^1H and ^{13}C NMR, UV−vis, ESI-MS spectrometry and by single crystal and powder X-ray diffraction.

Scheme 1. Synthetic Route of the Ligand S1 and Its Potential Recognition Sites Generating a Ω-Shape

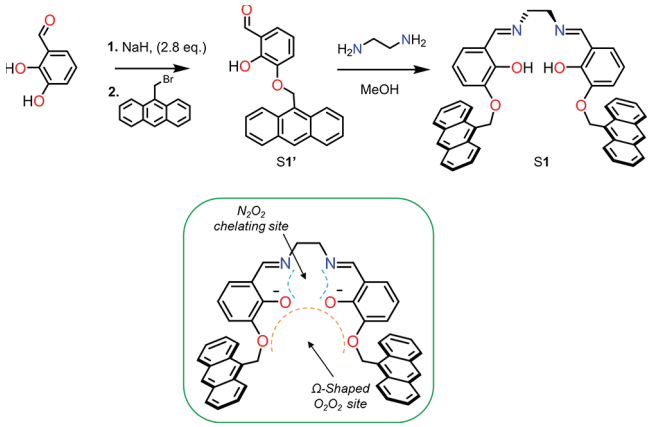

The self-assembling of the two anthracene moieties upon the coordination of certain metal cations is expected to induce a strong A–A* excimer fluorescence.[68] Indeed, containing a N_2O_2 imine-based coordinating site, the ligand **S1** can bind transition metal ions upon deprotonation. The coordination of the N_2O_2 moiety preorganizes the ligand in a Ω-shape, offering thus a second recognition site, O_2O_2, for the coordination of a second metal ion (Scheme 1). The coordination of a second metal ion at the O_2O_2 site becomes favorable and is expected to further modify the previous architecture, altering in turn the luminescence by bringing the fluorophores close to each other. Indeed, changing the degrees of freedom (mobility) of the molecular scaffold, receptor **S1** could have the ability to produce an excimer emission by metal ion-induced fluorescence.

Colorimetric Sensing of $Fe^{2+/3+}$. The coordination of Fe^{2+} and Fe^{3+} ions by **S1** (40 μM) leads to a coloration of the solution in red brown. This feature is the result of the establishment of broad CT bands in the 450–700 nm spectral window. One of them was assessed to be a metal-to-ligand charge transfer (MLCT) from a t_{2g} *d*-orbital of Fe^{2+} to the π* antibonding orbital on the N_2O_2 site, leading to the oxidation of the metallic center.[69] The other band was described as a ligand-to-metal charge transfer (LMCT) from a π-orbital of N_2O_2 to the e_g unoccupied *d*-orbital of Fe^{3+}, leading to the reduction of the metal.[70−72] The absorption coefficients (ε) were determined to be 2900 and 4300 M^{-1} cm^{-1}, respectively. Although the spectral features are similar for these two metal ions, the CT bands appeared to be more intense for Fe^{3+}. To exclude any interference in Fe^{2+} sensing by Fe^{3+}, the experiments were additionally carried out under anaerobic conditions, avoiding thus the potential oxidation of Fe^{2+} into Fe^{3+} by O_2 (Figure S3). Similar UV–vis spectral features have been observed under these conditions.

The Fe^{2+}/Fe^{3+} binding properties of **S1** were then investigated by UV–vis titrations. Upon the addition of increasing amounts of Fe^{3+} ($Fe(NO_3)_3$) or Fe^{2+} ($Fe(ClO_4)_2$), the characteristic absorption band at 366 nm is slightly red-shifted by 3 nm, giving rise to two isosbestic points at 385 and 389 nm (Figure 1A).

The corresponding binding isotherm curve shows a plateau after 1 equiv of Fe^{2+}/Fe^{3+} was added, indicating the formation of a 1:1 complex. This binding stoichiometry is then confirmed by a Job plot analysis which exhibits a maximum at 0.5 attesting the formation of a 1:1 complex in both cases (Figure S4–S5). The stoichiometry is supported by mass spectrometry for the Fe^{3+} compound with *m*/*z*: 734.19 $[M - NO_3]^+$ where $M([(FeS1 - 2H) + NO_3]) = 796.12$, Figure S6. (The Fe^{2+}-complex oxidizes rapidly in air). Moreover, a ^1H NMR titration of **S1** by Fe^{3+} and Fe^{2+} salts has been performed, showing a complete disappearance of the signals for the OH-group upon the addition of 1 equiv of Fe^{3+} or Fe^{2+} ions. This confirms the participation of O atoms (Figure S7–S8) of the N_2O_2 chelating site in the iron coordination. For both Fe^{2+}- and Fe^{3+}-**S1** complexes, the proton signal becomes broader upon metal ion addition, preventing an accurate titration of the complexes. This phenomenon indicates that the Fe^{2+}-complex is high spin, while in the case of Fe^{3+}, no conclusion can be drawn from NMR data as both high and low spin states give paramagnetic species.

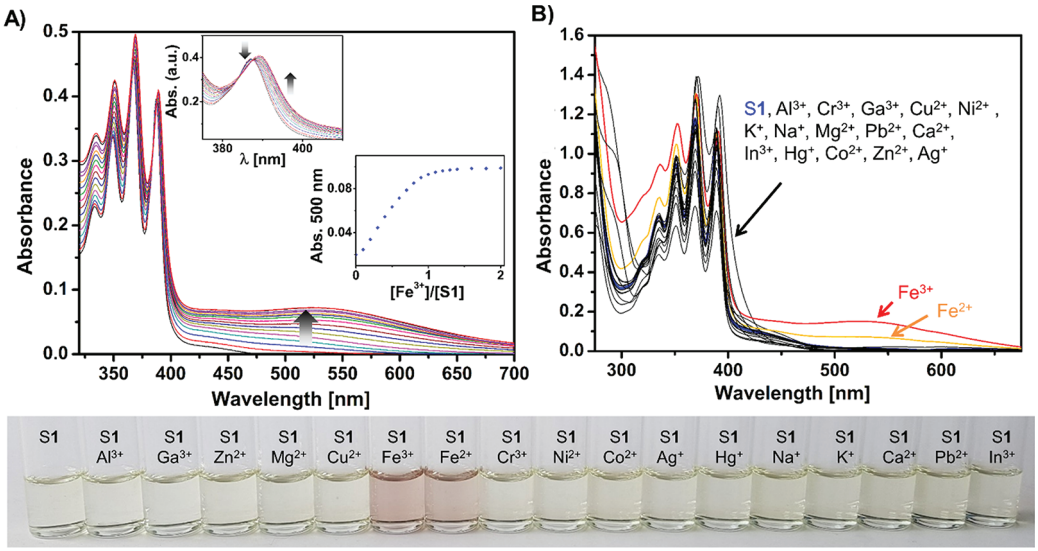

Figure 1. (A) UV–vis titration of **S1** (40 μM) by $Fe(NO_3)_3$ (0 to 80 μM) in DMF. The insets depict a zoom of the 370–420 nm window and the corresponding binding isotherm curve (λ = 530 nm). (B) UV–vis spectrum and color of **S1** solutions (100 μM in DMF) upon the addition of 1.2 equiv (120 μM) of different metal ions.

Scheme 2. Suggested Coordination Modes of the Sensor S1. (A) Coordination of Fe^{2+} or Fe^{3+} Ions by S1 Leading to the Establishment of a Broad CT Band, Giving Rise to a Red Brown Color. (B) Coordination of In^{3+} Ions by S1 Leading to the Self-Assembling of the Anthracene Moieties, Giving Rise to a Strong Excimer Emission

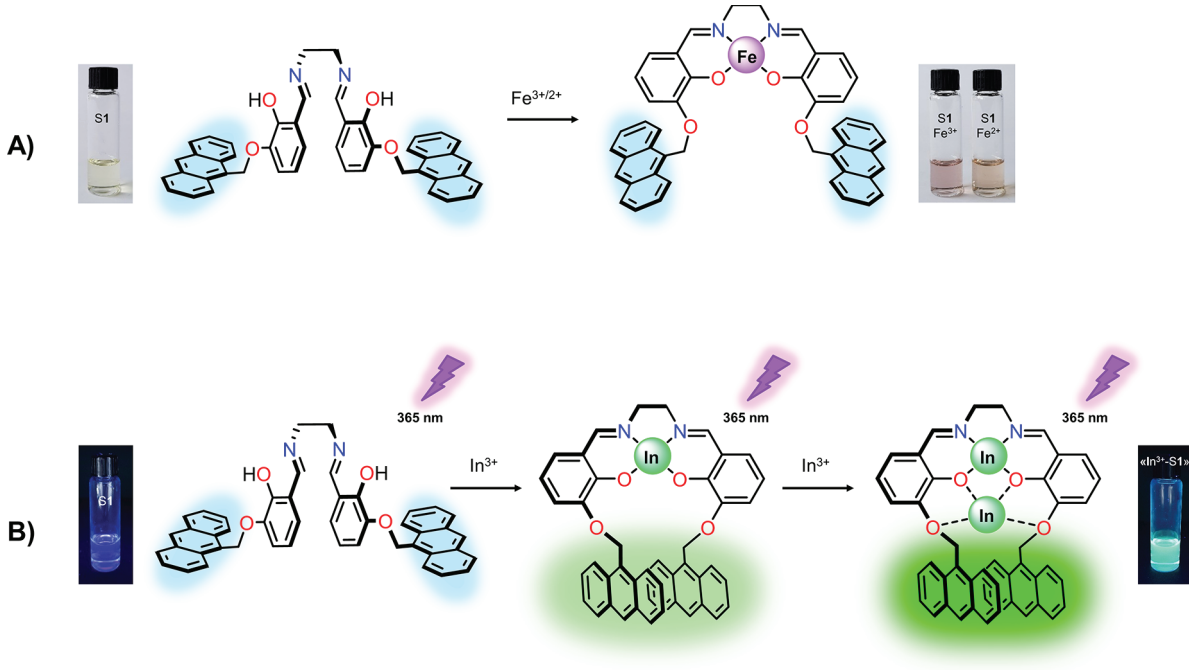

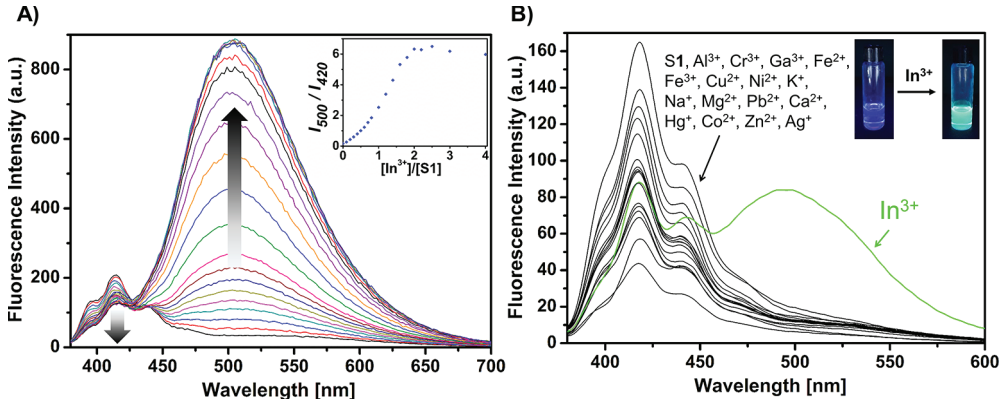

Figure 2. (A) Spectrofluorimetric titration of **S1** (40 μM) by $In(NO_3)_3$ (0 to 240 μM) in DMF (λ_{ex}= 365 nm). The inset depicts the corresponding binding isotherm curve by plotting the relative fluorescence intensity (I/I_0) changes (λ_{em} = 508 nm). (B) Selective detection of In^{3+} by sensor **S1**. Fluorescence emission spectra (λ_{ex} = 365 nm) of **S1** (40 μM in DMF) upon the addition of 1.2 equiv (48 μM) of different metal ions (detailed labeling of the fluorescence intensity depending on the used metal ion can be found in the Supporting Information, Figure S11).

The suggested coordination mechanism involves a twisted arrangement of the anthracene moieties impeding sterically the coordination of the O_2O_2 recognition site by a second cation (Scheme 2A). Therefore, the sensing ability of other metal ions has been determined by monitoring the potential CT transitions in the visible range after the addition of each metal ion. The absence of the latter broad band confirms that sensor **S1** can be used as a colorimetric chemosensor able to selectively sense Fe^{3+} or Fe^{2+} among other cations (Ag^+, Al^{3+}, Ga^{3+}, In^{3+}, Zn^{2+}, Cu^{2+}, Mg^{2+}, Cr^{3+}, Co^{2+}, Ni^{2+}, Na^+, K^+, Ca^{2+}, and Pb^{2+}) by colorimetry (Figure 1B). The calculation of detection limit (LOD) was then performed through standard deviations and linear fittings, giving a result of 0.44 μM for Fe^{3+} and 0.69 μM for Fe^{2+} (Figure S9–S10).

Fluorimetric Sensing of In^{3+}. Initially, after an excitation at 365 nm, receptor **S1** exhibits a weak monomer emission in the 375–475 nm range with a maximum at 420 nm. This might be explained by a photoinduced electron transfer (PET) which takes place from the nitrogen atoms of the imine groups to the fluorophore moieties, leading to fluorescence quenching.[73] The subsequent coordination of In^{3+} by **S1** generates an intense excimer emission in the 475–600 nm range with a maximum at 508 nm (λ_{ex} = 365 nm), probably via a parallel self-assembly of the two anthracene moieties through π–π stacked dimer interactions, leading to a bright green fluorescence (Figure 2A).[74−76] Concomitantly, a strong decrease of the typical monomer emission band is observed.

The binding mode was then analyzed by performing a spectrofluorimetric titration of **S1** by In^{3+}. This titration showed an increase of the excimer emission until 2 equiv of In^{3+} added. In the corresponding binding isotherm curve obtained by plotting the relative fluorescence intensity (I/I_0)

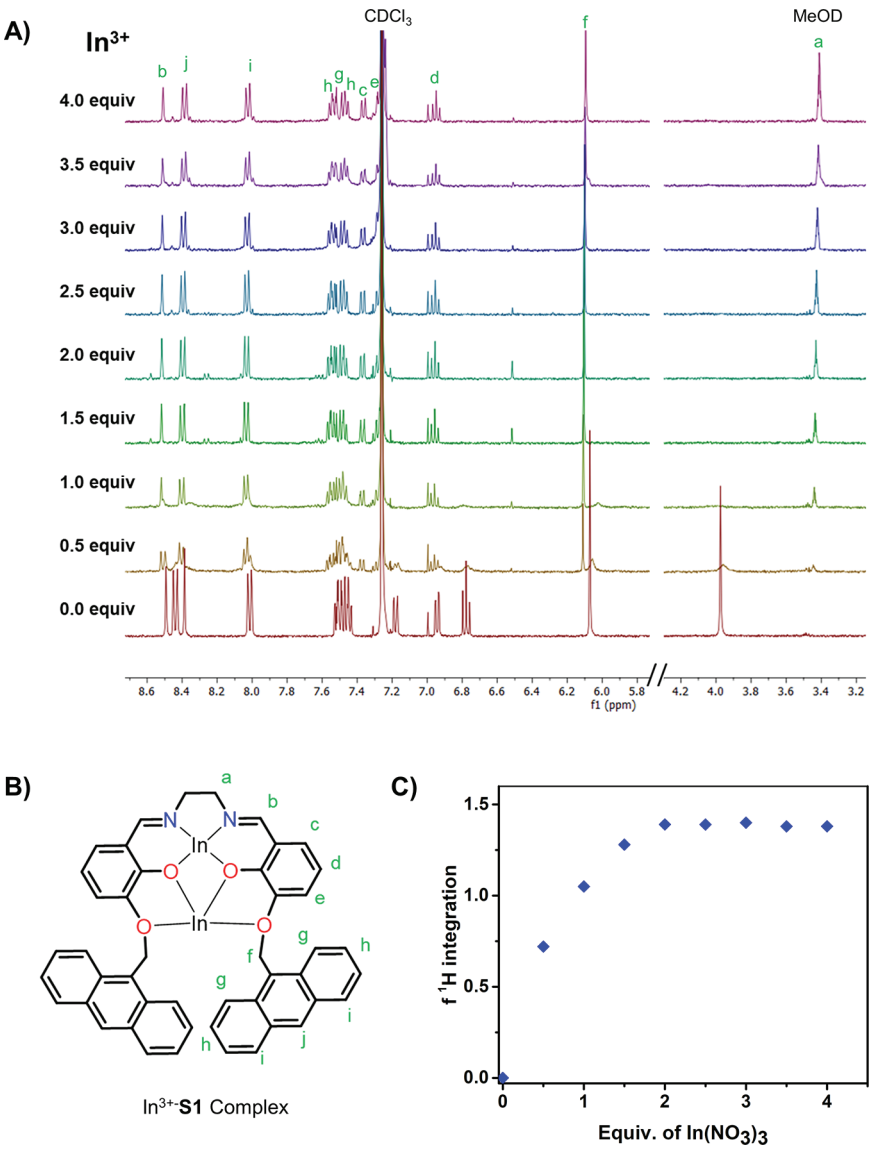

Figure 3. (A) Aromatic region of the ^{1}H NMR titration of **S1** with $In(NO_3)_3$ (in MeOD) forming the corresponding In^{3+}-**S1** complex at room temperature (0.5 mM) in $CDCl_3$. (B) ^{1}H NMR proton signals assignation of the complex assignation. (C) ^{1}H NMR titration binding isotherm of the In^{3+}-**S1** complex formation focused on the methylene-CH_2 bridge integrals, taking TMS as reference.

changes as a function of the metal concentration, a plateau is reached after the addition of 2 equiv of metal ion, revealing the formation of a 2:1 complex (Figure S12). This result also indicates the formation of the excimer conformation already after the coordination of the first In^{3+} ion within the N_2O_2 site (Scheme 2B) and displays thus a ratiometry with an isoemissive point at 428 nm (λ_{ex}= 365 nm). The calculation of detection limit (LOD) was performed through standard deviations and linear fittings yielding 0.53 μM (Figure S13).

Together with the Job plot result from fluorescence titration, which presents a maximum at around 0.35, the ESI-MS analysis also indicates the formation of a 2:1 complex (m/z: 1095.03 $[M\text{-}NO_3]^+$ where $M([(In_2\mathbf{S1} - 2H) + 4NO_3])$ = 1156.03, Figure S14). Additionally, a ^{1}H NMR titration of **S1** by In^{3+} ions in $CDCl_3$ has been carried out in order to confirm the complex stoichiometry. The perturbation of the **S1** ^{1}H NMR spectrum upon the addition of In^{3+} suggests a drastic reorganization and distortion of the ligand backbone during the complex formation, probably similar to what is observed in single crystal structures of 1:1 salen-type indium complexes.[66] For instance, the initial aromatic and methylene bridge signals disappear in favor of new shifted signals that appear during the titration, showing the formation of a new species in slow exchange regime (Figures 3A and 3B). The splitting of the anthracene external mutliplet signal at 7.5 ppm reflects the formation of an asymmetrical complex which is stabilized after the addition of 2 equiv of In^{3+} added. The shift of the methylene bridge-CH_2 singlet from 6.07 to 6.12 ppm also follows this tendency and confirms the 2:1 stoichiometry of the complex. Indeed, the binding isotherm of the complex formation established based on the methylene bridge-CH_2 signal appearing at 6.12 ppm, taking tetramethylsilan (TMS) as reference, shows a plateau after the addition of 2 equiv of In^{3+} ions (Figure 3C) (More details of the ^{1}H NMR titration can be found in the Supporting Information, Figures S15–S16). In addition, a ^{1}H NMR titration of **S1** by In^{3+} ions has been performed in DMSO displaying the complete deprotonation of the −OH groups, validating the contribution of oxygen atoms

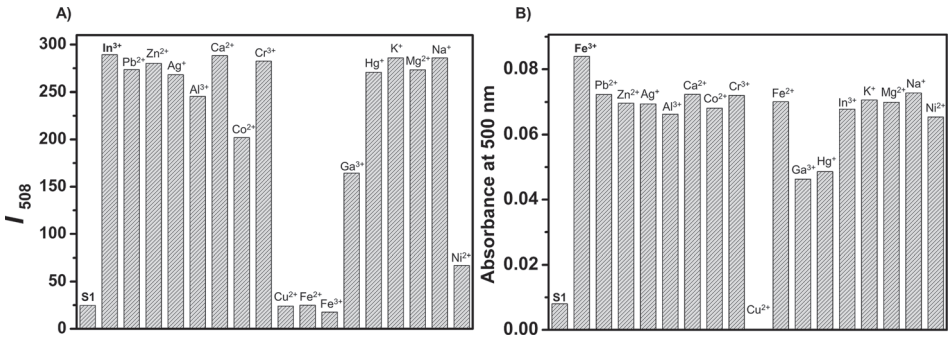

Figure 4. (A) Selectivity of **S1** (40 μM) toward In^{3+} (88 μM, 2.2 equiv) in the presence of other metal ions (88 μM, 2.2 equiv) in DMF (λ_{ex} = 365 nm, λ_{em}= 508 nm). (B) Selectivity of S1 (40 μM) toward Fe^{3+} (48 μM, 1.2 equiv) in the presence of other metal ions (48 μM, 1.2 equiv) in DMF (λ = 500 nm).

(from the N_2O_2 chelating site) in the complex formation (Figure S17).

Altogether, these results suggest that the chelation of one In^{3+} ion in the first N_2O_2 recognition site of the ligand brings the anthracene moieties into close enough proximity to start the formation of the excimer A–A* in the sensing mechanism. However, the overall structure is subsequently rigidified upon complexation of the second In^{3+} ion, amplifying thus the excimer emission in solution (Scheme 2B).

The lack of a single crystal X-ray structure prevents the exact characterization of the coordination compound. Nevertheless, several previously described salen-based indium complexes provide valuable examples of different possible coordination modes. Indeed, some reported indium structures[65,77,78] allow us to state that the reaction of **S1** with one In^{3+} could give rise to a distorted square pyramidal coordination of In^{3+} by the N_2O_2 chelating moiety of **S1** (formed by two phenolate moieties and two imine groups) with an axial oxygen donor atom from a nitrate ion. This will likely enhance the nonplanarity of the ligand as it wraps around a metal ion that is too large to perfectly fit into the N_2O_2 cavity. For the second indium ion, it is suggested to be coordinated by all four oxygen atoms of the O_2O_2 compartment of the ligand. Similarly to a few similar structures reported earlier,[79] it is proposed that the coordination sphere of the second metal ion is completed by two O atoms of two nitrate ions in axial positions. The presence of a complex dimer or 1D coordination polymers can be discussed via bridging nitrate or solvent ligands; however, this phenomenon seems to be less probable due to the steric hindrance of the two anthracene moieties and the fact that no evidence of such species or oligomers was observed by ESI-MS analysis. In total, one 2–-charged ligand and three nitrate anions would thus be coordinated directly to the indium ions, while an additional anion may not directly be coordinated to the complex. This situation would perfectly fit to the observed mass spectra.

The binding capacity of sensor **S1** for diverse metal ions was also studied by spectrofluorimetry, showing however no excimer formation. This specific behavior allows sensor **S1** to detect and discriminate In^{3+} from all other metal ions tested (Ag^+, Al^{3+}, Ga^{3+}, Zn^{2+}, Cu^{2+}, Fe^{3+}, Fe^{2+}, Mg^{2+}, Cr^{3+}, Co^{2+}, Ni^{2+}, Na^+, K^+, Ca^{2+}, and Pb^{2+}) by fluorometry (Figure 2B). The excimer emission is not produced by the coordination of other cations due to the lack of an efficient distortion of the **S1**'s backbone, avoiding thus the excimer formation.

Compared to other 3+ charged, yet smaller, metal ions such as Al^{3+} (ionic radius 67.5 pm) or Ga^{3+} (76 pm), In^{3+} is the only one generating an excimer emission. Furthermore, the interaction of **S1** with lanthanide ions such as Er^{3+} (103 pm) or Eu^{3+} (108 pm), which are bigger than In^{3+}, has been qualitatively studied and also no optical response has been observed. This phenomenon is likely due to the "optimum" size of the indium ion to induce the excimer formation from the two anthracene moieties of the ligand.[66] Crystal structures of salen-type ligands with smaller metal ions do not lead to a strong deformation of the salen backbone on one hand,[80] while larger ones may not fit well into the N_2O_2 chelating site.[81,82] This may then possibly lead to sandwich-type complexes with two ligands per cation, binding via N_2O_2-entities like in the case of Tb^{3+}[83,84] or protonation of the N-donor atoms and binding via the O_2O_2 entity only, as for Ln^{3+},[85] preventing thus the excimer formation, respectively offering quenching pathways. This allows us to argue that indium possesses the "optimal size", resulting in a strong excimer emission generating from the perfect arrangement of the anthracene moieties.

Competition Studies. In order to challenge the robustness of the sensor, potential interference from other ions in the detection of Fe^{2+}/Fe^{3+} and In^{3+} was investigated in the presence of other competitive ions, in particular Ag^+, Al^{3+}, Ga^{3+}, Zn^{2+}, Cu^{2+}, Fe^{2+}, Fe^{3+}, In^{3+}, Mg^{2+}, Cr^{3+}, Co^{2+}, Ni^{2+}, Na^+, K^+, Ca^{2+}, and Pb^{2+}. These cations were added to a solution of **S1** (40 μM) before the addition of equivalent amounts of In^{3+}or Fe^{2+}/Fe^{3+} (2 and 1 equiv, 88 μM and 48 μM, respectively) (Figures S18–S20).

In the case of In^{3+}, the experiment was performed by monitoring the excimer emission of the In^{3+}-**S1** complex. Most of the present cations did not interfere with the detection of In^{3+} except three of them, Cu^{2+}, Fe^{2+}, and Fe^{3+}, which inhibited the indium sensing considerably (Figure 4A). Indeed, after the coordination of these three metal ions by **S1**, no subsequent excimer emission band was observed upon In^{3+} addition even though a decrease of the monomer emission has been observed. Cu^{2+} and Fe^{3+} are well-known paramagnetic ions with an incompletely filled *d* shell. These cations have been described to strongly quench the fluorescence of the fluorophore by electron or energy transfer.[86–88] Moreover, the coordination of Cu^{2+}, Fe^{2+}, or Fe^{3+} ions by **S1** would also prevent the assembly of the anthracene moieties, avoiding the In^{3+}-induced excimer emission. Therefore, the formation of these three different complexes decreases the monomer emission fluorescence of **S1** and impedes the formation of the excimer upon the addition of In^{3+} ions (Figure S20).

Scheme 3. Suggested Recognition Mechanism of Fe^{2+}, Fe^{3+}, and Cu^{2+} Ions by the In^{3+}-S1 Complex

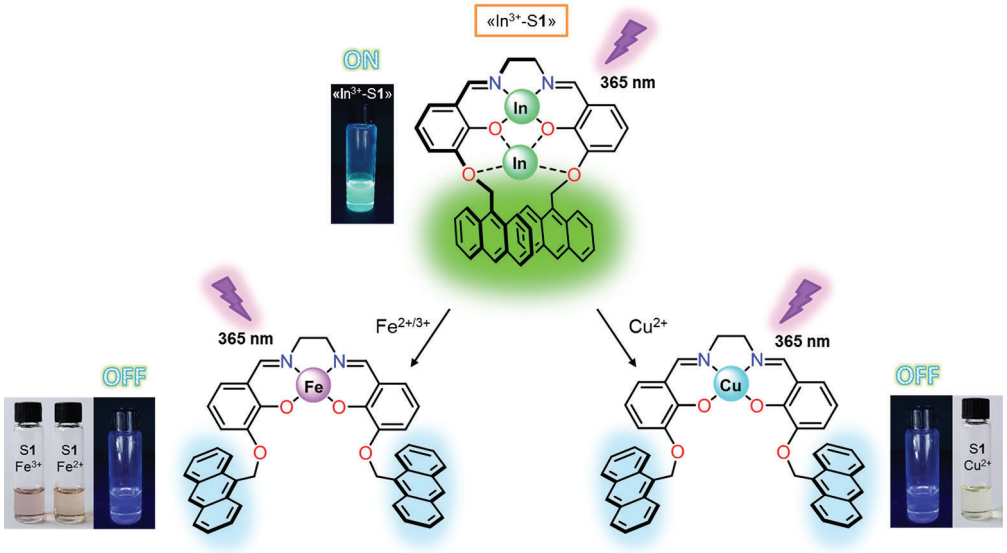

For Fe^{3+} and Fe^{2+}, similar competition experiments were performed by monitoring the typical broad absorption band of the Fe^{2+}- or Fe^{3+}-**S1** complex upon the addition of the challenging cations. In this case, Cu^{2+} ions were the only cations able to interfere with the detection of Fe^{2+}/Fe^{3+} (Figures S19 and 4B). Indeed, when Cu^{2+} was preliminarily added to the solution, no color change and respectively no appearance of the broad CT band were observed upon the subsequent addition of Fe^{2+} or Fe^{3+} (Figure S18–S19).

These results suggest a stronger binding of Cu^{2+} compared to the other cations, suggesting a binding strength tendency: Cu^{2+} > Fe^{3+} > Fe^{2+} > In^{3+}. However, the binding constant could not be accurately determined, due to a too high affinity of **S1** for these cations. A study of Cu^{2+} complexation by sensor **S1** revealed a 1:1 stoichiometry (Figure S21). Although this higher affinity for Cu^{2+} limits the sensing of In^{3+} and Fe^{2+}/Fe^{3+} to copper-free media, it also expands the sensing ability of the probe, able to detect and discriminate Fe^{2+}/Fe^{3+} and Cu^{2+} ions when used in the form of the In^{3+}-**S1** complex as "on–off" sensor. Indeed, the In^{3+}-**S1** complex can be hence used as a switch-off fluorescent probe for Cu^{2+} and Fe^{2+}/Fe^{3+} detection, which subsequently discriminates these metal ions by colorimetry upon the formation of the Fe^{2+}- or Fe^{3+}-**S1** complex (Scheme 3).

Solvent Effect Studies. The behavior of **S1** has been investigated in common solvents by UV–vis and spectrofluorimetric measurements. The fluorescence emission spectrum of the ligand **S1** upon excitation at 365 nm exhibits the characteristic monomer emission of the anthracene moiety in all tested conditions. However, the excimer emission appeared to be strongly dependent on the solvent system used.[89]

Figure 5 shows a clear enhancement of the excimer formation in less polar solvents such as toluene, THF, or DCM. By increasing the polarity of the solvents, the In^{3+}-**S1** complex displays a decrease of the emission presumably due to nonradiative relaxation and solvent interactions inducing a lack of flexibility within the sensor and inhibiting the excimer formation.[90,91] For instance, in pure DMSO as well as in a mixture of DMSO with 5% of buffer (Bis-Tris, 10 mM, pH 7), the addition of In^{3+} to the solution of **S1** resulted only in a slight excimer emission. In contrast, the fluorescence emission

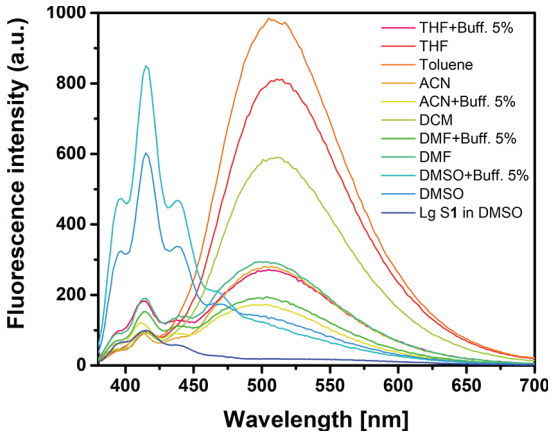

Figure 5. Solvent dependency of the fluorogenic detection of In^{3+} (40 μM) in DCM, THF, DMF, DMSO, ACN, toluene, and their corresponding buffer (5%, Bis-Tris, 10 mM, pH 7) mixtures.

spectra of the In^{3+}-**S1** complex in the other solvents and their respective buffer mixtures exhibit a broad excimer emission band, reducing drastically the monomer emission band. In DCM, THF, or toluene, this effect is even more pronounced, increasing the excimer emission band intensity and decreasing almost totally the monomer emission band. Therefore, the In^{3+} sensing is less effective in DMSO than in other solvent systems, even though a slight excimer emission band can be detected. These results showed a clear dependency of the In^{3+}-**S1** excimer formation as a function of the solvent used (Figure 5). Moreover, the presence of the buffer leads in general to a weaker emission than in the absence of buffer. This might be due to the interaction of the buffer with the ligand, e.g. via H-bonds, and hence additional quenching pathways.

The Fe^{2+}/Fe^{3+} detection is however not dependent on the solvent system. Indeed, the characteristic broad CT band appearing upon Fe^{2+}/Fe^{3+} addition has been observed in all tested solvents (Figure 6).

These results revealed that the use of different solvents does not interfere with the detection of Fe^{2+}/Fe^{3+} and In^{3+}, despite the low efficiency of the In^{3+} detection in DMSO and in its buffer mixtures. These measurements also showed that the use

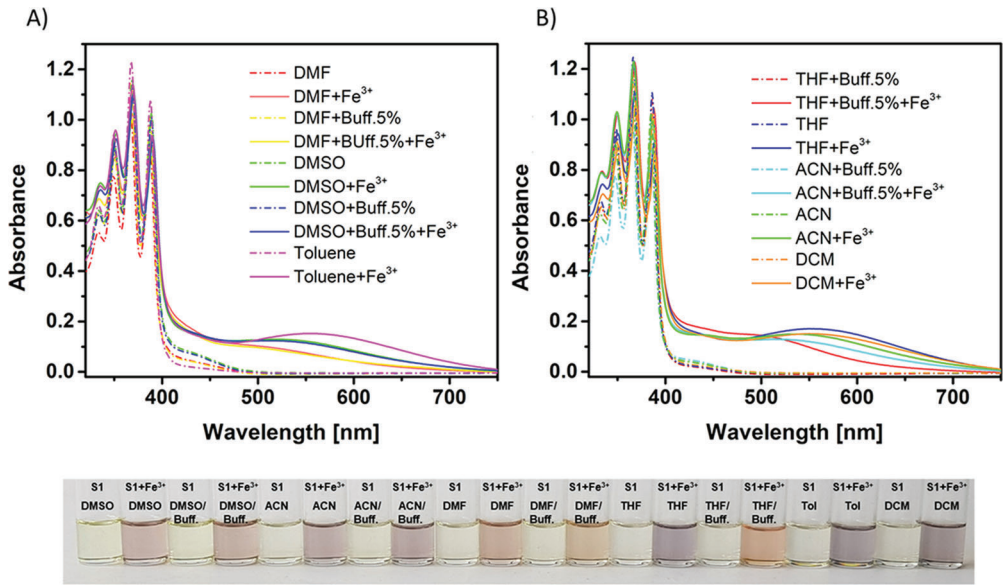

Figure 6. Solvent dependency of the colorimetric detection of Fe^{3+} (40 μM) in (A) DMF, DMSO, and toluene and in (B) THF, ACN, DCM, and their correspondent buffer (5%, Bis-Tris, 10 mM, pH 7) mixtures.

of buffer in diverse solvents is also possible in order to target potential biological assays.

Crystallography. In order to gain further insights into the coordination mechanisms of metal ions by **S1**, considerable efforts were undertaken to obtain good quality single crystals of the host–guest complexes. This was however only possible for compound **S1′**, the ligand **S1**, and the 1:1 Cu^{2+}-**S1** complex.

For **S1**, having a C_2-axis running through the geometrical middle of the central C–C bond of the molecule, the two anthracene moieties point outward with the chromophore planes nearly perpendicular to the dioxo-benzene rings with an angle of 85° (Figure 7). These latter two dioxo-benzene rings

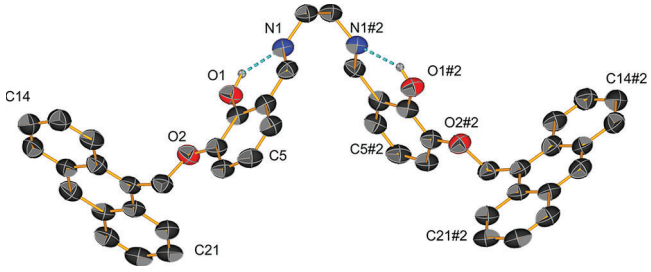

Figure 7. Crystal structure of sensor **S1**, (#2(1/2 − x, 1/2 − y, z)); H atoms are omitted except for O1–H and O1#2-H (thermal ellipsoids at 50% probability level).

are arranged in an antiparallel fashion forming an angle of 70°, probably due to the steric hindrance of the two chromophores. This arrangement is stabilized by the H-bonds between the alcohol proton H1 and the N atom N1 (and their symmetry equivalents), with a distance of 1.947 Å.

In the Cu^{2+}-**S1** complex, the molecule of **S1** is now deprotonated and wraps around the Cu^{2+} cation, which occupies the N_2O_2 chelating site of the ligand in a quasi-perfect square planar fashion (Figure 8). Having a bond valence sum[92] of nearly 2.0 provided by the N_2O_2 cavity of the sensor, Cu^{2+} does not need to complete its coordination sphere using additional solvent or anion entities. The angle sum around the metal ion within the N_2O_2 recognition moiety is

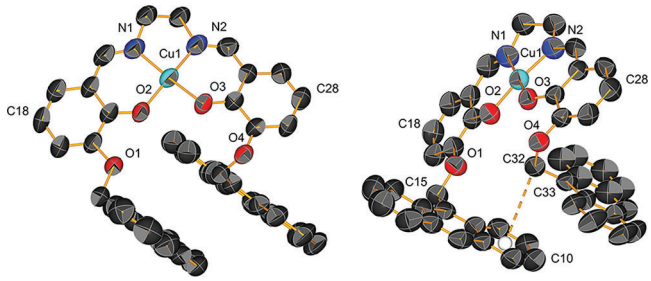

Figure 8. Two views of the crystal structure of the complex Cu^{2+}-**S1**, all H atoms are omitted for clarity (thermal ellipsoids at 50% probability level).

360.85°, indicating the quasi planarity of this coordination. Compared to the structure of **S1** alone, the orientation of one side arm of the complex is almost preserved with an angle of 79.40° between the external anthracene moiety and the main plane formed by the dioxo-benzene ring. For the other extremity of the ligand, the anthracene moiety points toward the benzene ring with an angle of 64.44°, inducing a slight distortion of the planarity of the N_2O_2 coordination of 20.03° based on the mean aromatic ring planes. The two anthracene moieties are in parallel planes; however, they do not stack on top of each other, showing closest contacts via C32– π and C10 – C33 at 3.584 and 3.534 Å, respectively. Access to the O_2O_2 cavity seems thereby hindered by the large hydrophobic groups, one of which points above, and the other below that binding site. A detailed description of all single crystal structures and their corresponding figures can be found in the Supporting Information (Figures S22–S24 and Table S1).

The structural aspects of this Cu complex of **S1** allow us to conclude that the binding of a metal ion to the first coordination site, N_2O_2, apparently induces a steric hindrance of the anthracene moieties within the Cu^{2+} complex. This binding restricts thus the access to the second recognition site, O_2O_2, inhibiting the coordination of a potential second cation and impeding the correct self-assembly of the anthracene moieties. From the above solution studies, we assume that the ligand will adopt a similar behavior in the presence of iron,

while a distinct arrangement of the probe in contact with indium seems to occur. Indeed, solid state structures of Schiff base derived ligands with indium show a ca. 10° greater folding deformation of the ligand scaffold than for transition metal ions such as Cu^{2+}.[65,66] Therefore, the coordination of the first indium ion to the probe **S1** might lead to a parallel arrangement of the anthracene moieties on one side of the O_2O_2 cavity, as indicated by the excimer formation, thereby giving access to the O_2O_2 cavity and thereby rendering the coordination of a second indium ion possible.

CONCLUSION

A highly versatile sensor has been successfully synthesized and introduced as first selective chromogenic and fluorogenic sensor for iron and indium ions. Probe **S1** is able to detect In^{3+} ions exhibiting strong excimer emission in various common solvents. Moreover, the designed compound can also be employed as selective sensor to detect the presence of Fe^{2+} or Fe^{3+} ions. In both cases, competition experiments in the presence of other cations demonstrated that the Cu^{2+} ion prevents the excimer emission of the two anthracene moieties of the sensor **S1** and impedes the color change of the solution. This effect may lead to the formation of a potential new sensor, the In^{3+}-**S1** complex, which could be used as "On−Off" fluorogenic sensor for the detection of Cu^{2+} and Fe^{2+}/Fe^{3+}, subsequently distinguishable by colorimetry. Moreover, the obtainment of the ligand crystal structure and its Cu-complex helped to interpret the different detection mechanisms. This new anthracene-functionalized Schiff-base probe **S1**, which exhibits very low detection limits for the sensing of In^{3+} and Fe^{2+}/Fe^{3+} ions in various solvent systems, could be used in the tracking of environmental In^{3+} and Fe^{2+}/Fe^{3+} ions and *in vitro* biological samples. It could then also provide inspiration for the design and development of new hydrosoluble sensors for such detection *in vivo*.

ASSOCIATED CONTENT

Supporting Information

The Supporting Information is available free of charge on the ACS Publications website at DOI: 10.1021/acs.inorgchem.9b01478.

General experimental information; NMR spectrum of the aldehyde based starting material **S1′** and of the ligand **S1**; NMR titration of the probe **S1**; UV−vis and fluorescent titrations of sensor **S1**; ESI mass analysis for Fe^{2+}, Fe^{3+}, and In^{3+} complex; Competition experiments; Detection limits of Fe^{2+}, Fe^{3+}, and In^{3+}; Fe^{2+} and Fe^{3+} oxidation test; Crystallographic data (PDF)

Accession Codes

CCDC 1860984−1860986 contain the supplementary crystallographic data for this paper. These data can be obtained free of charge via www.ccdc.cam.ac.uk/data_request/cif, or by emailing data_request@ccdc.cam.ac.uk, or by contacting The Cambridge Crystallographic Data Centre, 12 Union Road, Cambridge CB2 1EZ, UK; fax: +44 1223 336033.

AUTHOR INFORMATION

Corresponding Author

*E-mail: Katharina.fromm@unifr.ch.

ORCID

Alba Finelli: 0000-0002-0273-9613

Nelly Hérault: 0000-0001-8986-7759

Cheal Kim: 0000-0002-7580-0374

Katharina M. Fromm: 0000-0002-1168-0123

Author Contributions

The manuscript was written through contributions of all authors. All authors have given approval to the final version of the manuscript.

Notes

The authors declare no competing financial interest.

ACKNOWLEDGMENTS

A.F. is grateful to Noémie Voutier for fruitful discussions. This work was supported by the Swiss National Science Foundation (grant number 200020_152777) and the National Research Foundation of Korea through a "Bilateral Korean-Swiss Science and Technology Program", by Frimat and the University of Fribourg.

REFERENCES

(1) Oakley, A. E.; Collingwood, J. F.; Dobson, J.; Love, G.; Perrott, H. R.; Edwardson, J. A.; Elstner, M.; Morris, C. M. Individual dopaminergic neurons show raised iron levels in Parkinson disease. *Neurology* **2007**, *68*, 1820−1825.

(2) Bishop, G. M.; Robinson, S. R.; Liu, Q.; Perry, G.; Atwood, C. S.; Smith, M. A. Iron: a pathological mediator of Alzheimer disease? *Dev. Neurosci.* **2002**, *24*, 184−187.

(3) Rapp, R. A. The transition from internal to external oxidation and the formation of interruption bands in silver-indium alloys. *Acta Metall.* **1961**, *9*, 730−741.

(4) Stanbery, B. J. Copper indium selenides and related materials for photovoltaic devices. *Crit. Rev. Solid State Mater. Sci.* **2002**, *27*, 73−117.

(5) Nagano, K.; Nishizawa, T.; Umeda, Y.; Kasai, T.; Noguchi, T.; Gotoh, K.; Ikawa, N.; Eitaki, Y.; Kawasumi, Y.; Yamauchi, T. Inhalation carcinogenicity and chronic toxicity of indium-tin oxide in rats and mice. *J. Occup. Health* **2011**, *53*, 175−187.

(6) Lokanc, M.; R. Eggert, M. R. *The Availability of Indium: The Present, Medium Term, and Long Term*; 2015.

(7) Lim, C. H.; Han, J.-H.; Cho, H.-W.; Kang, M. Studies on the toxicity and distribution of indium compounds according to particle size in Sprague-Dawley rats. *Toxicol. Res.* **2014**, *30*, 55.

(8) Castronovo, F. P.; Wagner, H. N. Factors affecting the toxicity of the element indium. *Br. J. Exp. Pathol.* **1971**, *52*, 543.

(9) Clarkson, T. W.; Friberg, L.; Nordberg, G. F.; Sager, P. R. *Biological monitoring of toxic metals*; Springer Science & Business Media, 2012; ISBN 1461309611.

(10) Harvey, R. R.; Virji, M. A.; Cummings, K. J. Assessing risk of indium lung disease to workers in downstream industries. *Am. J. Ind. Med.* **2017**, *60*, 310.

(11) Choi, S.; Won, Y. L.; Kim, D.; Lee, M.; Choi, Y. j.; Park, J.; Kim, H.; Jung, J. I.; Lee, S.; Kim, E. Interstitial lung disorders in the indium workers of Korea: an update study for the relationship with biological exposure indices. *Am. J. Ind. Med.* **2015**, *58*, 61−68.

(12) Suzuki, Y.; Matsushita, H. Interaction of metal ions with phospholipid monolayer and their acute toxicity. *Ind. Health* **1969**, *7*, 143−154.

(13) Bi, X.; Westerhoff, P. Adsorption of III/V ions (In(III), Ga(III) and As(V)) onto SiO_2, CeO_2 and Al_2O_3 nanoparticles used in the semiconductor industry. *Environ. Sci.: Nano* **2016**, *3*, 1014−1026.

(14) Stellman, J. M. *Encyclopaedia of occupational health and safety*; International Labour Organization, 1998; Vol. *1*; ISBN 9221092038.

(15) Chapin, R. E.; Harris, M. W.; Hunter, E. S., III; Davis, B. J.; Collins, B. J.; Lockhart, A. C. The reproductive and developmental toxicity of indium in the Swiss mouse. *Toxicol. Sci.* **1995**, *27*, 140−148.

(16) Cummings, K. J.; Nakano, M.; Omae, K.; Takeuchi, K.; Chonan, T.; Xiao, Y.; Harley, R. A.; Roggli, V. L.; Hebisawa, A.; Tallaksen, R. J. Indium lung disease. *Chest* **2012**, *141*, 1512−1521.
(17) Shannon, R. D. Revised effective ionic radii and systematic studies of interatomic distances in halides and chalcogenides. *Acta Crystallogr., Sect. A: Cryst. Phys., Diffr., Theor. Gen. Crystallogr.* **1976**, *32*, 751−767.
(18) McIntyre, P. A.; Larson, S. M.; Eikman, E. A.; Colman, M.; Scheffel, U.; Hodkinson, B. A. Comparison of the metabolism of iron-labeled transferrin (Fe· TF) and indium-labeled transferrin (In· TF) by the erythropoietic marrow. *J. Nucl. Med.* **1974**, *15*, 856−862.
(19) Moshtaghie, A. A.; Ghaffari, M. A. Study of the binding of iron and indium to human serum apo-transferrin. *Iran. Biomed. J.* **2003**, *7*, 73−77.
(20) Wu, S.-P.; Chen, Y.-P.; Sung, Y.-M. Colorimetric detection of Fe^{3+} ions using pyrophosphate functionalized gold nanoparticles. *Analyst* **2011**, *136*, 1887−1891.
(21) Narayanaswamy, N.; Govindaraju, T. Aldazine-based colorimetric sensors for Cu^{2+} and Fe^{3+}. *Sens. Actuators, B* **2012**, *161*, 304−310.
(22) Jung, J. M.; Lee, S. Y.; Kim, C. A novel colorimetric chemosensor for multiple target metal ions Fe^{2+}, Co^{2+}, and Cu^{2+} in a near-perfect aqueous solution: Experimental and theoretical studies. *Sens. Actuators, B* **2017**, *251*, 291−301.
(23) Lee, M. H.; Van Giap, T.; Kim, S. H.; Lee, Y. H.; Kang, C.; Kim, J. S. A novel strategy to selectively detect Fe(III) in aqueous media driven by hydrolysis of a rhodamine 6G Schiff base. *Chem. Commun.* **2010**, *46*, 1407−1409.
(24) Wang, B.; Hai, J.; Liu, Z.; Wang, Q.; Yang, Z.; Sun, S. Selective Detection of Iron (III) by Rhodamine-Modified Fe_3O_4 Nanoparticles. *Angew. Chem., Int. Ed.* **2010**, *49*, 4576−4579.
(25) Kim, S. K.; Kim, S. H.; Kim, H. J.; Lee, S. H.; Lee, S. W.; Ko, J.; Bartsch, R. A.; Kim, J. S. Indium(III)-Induced Fluorescent Excimer Formation and Extinction in Calix[4]arene−Fluoroionophores. *Inorg. Chem.* **2005**, *44*, 7866−7875.
(26) Cho, H.; Chae, J. B.; Kim, C. A thiophene-based blue-fluorescent emitting chemosensor for detecting indium (III) ion. *Inorg. Chem. Commun.* **2018**, *97*, 171−175.
(27) Kim, C.; Chae, J. B. A Highly Selective Fluorescent Chemosensor for Detecting Indium (III) with a Low Detection Limit and its Application. *J. Fluoresc.* **2018**, *28*, 1363−1370.
(28) Wu, Y.-C.; Li, H.-J.; Yang, H.-Z. A sensitive and highly selective fluorescent sensor for In^{3+}. *Org. Biomol. Chem.* **2010**, *8*, 3394−3397.
(29) Jang, H. J.; Kang, J. H.; Yun, D.; Kim, C. A multifunctional selective "turn-on" fluorescent chemosensor for detection of Group IIIA ions Al^{3+}, Ga^{3+} and In^{3+}. *Photochem. Photobiol. Sci.* **2018**, *17*, 1247−1255.
(30) Okda, H. E.; El Sayed, S.; Otri, I.; Ferreira, R. C. M.; Costa, S. P. G.; Raposo, M. M. M.; Martínez-Máñez, R.; Sancenón, F. A simple and easy-to-prepare imidazole-based probe for the selective chromo-fluorogenic recognition of biothiols and Cu (II) in aqueous environments. *Dyes Pigm.* **2019**, *162*, 303−308.
(31) Lee, S. Y.; Yang, M.; Kim, C. A dual target chemosensor for the fluorometric detection of In^{3+} and colorimetric detection of Fe^{3+}. *Spectrochim. Acta, Part A* **2018**, *205*, 622−629.
(32) Kim, H.; Kim, K. B.; Song, E. J.; Hwang, I. H.; Noh, J. Y.; Kim, P.-G.; Jeong, K.-D.; Kim, C. Turn-on selective fluorescent probe for trivalent cations. *Inorg. Chem. Commun.* **2013**, *36*, 72−76.
(33) Han, D. Y.; Kim, J. M.; Kim, J.; Jung, H. S.; Lee, Y. H.; Zhang, J. F.; Kim, J. S. ESIPT-based anthraquinonylcalix[4]crown chemosensor for In^{3+}. *Tetrahedron Lett.* **2010**, *51*, 1947−1951.
(34) Mehta, P. K.; Hwang, G. W.; Park, J.; Lee, K.-H. Highly Sensitive Ratiometric Fluorescent Detection of Indium (III) Using Fluorescent Probe Based on Phosphoserine as a Receptor. *Anal. Chem.* **2018**, *90*, 11256−11264.
(35) Santos-Figueroa, L. E.; Llopís-Lorente, A.; Royo, S.; Sancenón, F.; Martínez-Máñez, R.; Costero, A. M.; S, G.; M, P. A Chalcone-Based Highly Selective and Sensitive Chromofluorogenic Probe for Trivalent Metal Cations. *ChemPlusChem* **2015**, *80*, 800−804.
(36) Wu, D.; Sedgwick, A. C.; Gunnlaugsson, T.; Akkaya, E. U.; Yoon, J.; James, T. D. Fluorescent chemosensors: the past, present and future. *Chem. Soc. Rev.* **2017**, *46*, 7105−7123.
(37) Zhou, X.; Lee, S.; Xu, Z.; Yoon, J. Recent progress on the development of chemosensors for gases. *Chem. Rev.* **2015**, *115*, 7944−8000.
(38) Formica, M.; Fusi, V.; Giorgi, L.; Micheloni, M. New fluorescent chemosensors for metal ions in solution. *Coord. Chem. Rev.* **2012**, *256*, 170−192.
(39) Gale, P. A.; Caltagirone, C. Fluorescent and colorimetric sensors for anionic species. *Coord. Chem. Rev.* **2018**, *354*, 2−27.
(40) Zhang, Z.; Lu, S.; Sha, C.; Xu, D. A single thiourea-appended 1, 8-naphthalimide chemosensor for three heavy metal ions: Fe^{3+}, Pb^{2+}, and Hg^{2+}. *Sens. Actuators, B* **2015**, *208*, 258−266.
(41) Hwang, S. M.; Kim, M. S.; Lee, M.; Lim, M. H.; Kim, C. Single fluorescent chemosensor for multiple targets: sequential detection of Al^{3+} and pyrophosphate and selective detection of F^- in near-perfect aqueous solution. *New J. Chem.* **2017**, *41*, 15590−15600.
(42) Song, E. J.; Kang, J.; You, G. R.; Park, G. J.; Kim, Y.; Kim, S.-J.; Kim, C.; Harrison, R. G. A single molecule that acts as a fluorescence sensor for zinc and cadmium and a colorimetric sensor for cobalt. *Dalt. Trans.* **2013**, *42*, 15514−15520.
(43) Xu, Z.; Xiao, Y.; Qian, X.; Cui, J.; Cui, D. Ratiometric and selective fluorescent sensor for Cu(II) based on internal charge transfer (ICT). *Org. Lett.* **2005**, *7*, 889−892.
(44) Zeng, L.; Miller, E. W.; Pralle, A.; Isacoff, E. Y.; Chang, C. J. A selective turn-on fluorescent sensor for imaging copper in living cells. *J. Am. Chem. Soc.* **2006**, *128*, 10−11.
(45) Yoon, S.; Miller, E. W.; He, Q.; Do, P. H.; Chang, C. J. A bright and specific fluorescent sensor for mercury in water, cells, and tissue. *Angew. Chem.* **2007**, *119*, 6778−6781.
(46) Chang, J. H.; Choi, Y. M.; Shin, Y. A significant fluorescence quenching of anthrylaminobenzocrown ethers by paramagnetic metal cations. *Bull. Korean Chem. Soc.* **2001**, *22*, 527−530.
(47) Palomares, E.; Vilar, R.; Durrant, J. R. Heterogeneous colorimetric sensor for mercuric salts. *Chem. Commun.* **2004**, *40*, 362−363.
(48) Kim, K. B.; Kim, H.; Song, E. J.; Kim, S.; Noh, I.; Kim, C. A cap-type Schiff base acting as a fluorescence sensor for zinc (II) and a colorimetric sensor for iron (II), copper (II), and zinc (II) in aqueous media. *Dalt. Trans.* **2013**, *42*, 16569−16577.
(49) Seth, P.; Ghosh, S.; Figuerola, A.; Ghosh, A. Trinuclear heterometallic Cu(II)-Mn(II) complexes of a salen type Schiff base ligand: anion dependent variation of phenoxido bridging angles and magnetic coupling. *Dalt. Trans.* **2014**, *43*, 990−998.
(50) Helal, A.; Rashid, M. H. O.; Choi, C.-H.; Kim, H.-S. Chromogenic and fluorogenic sensing of Cu^{2+} based on coumarin. *Tetrahedron* **2011**, *67*, 2794−2802.
(51) Hui, J. K.; Yu, Z.; MacLachlan, M. J. Supramolecular Assembly of Zinc Salphen Complexes: Access to Metal-Containing Gels and Nanofibers. *Angew. Chem., Int. Ed.* **2007**, *46*, 7980−7983.
(52) Kleij, A. W. Zinc-centred salen complexes: versatile and accessible supramolecular building motifs. *Dalt. Trans.* **2009**, *38*, 4635−4639.
(53) Bermejo, M. R.; Carballido, R.; Fernández-García, M. I.; González-Noya, A. M.; González-Riopedre, G.; Maneiro, M.; Rodríguez-Silva, L. Synthesis, Characterization, and Catalytic Studies of Mn(III)-Schiff Base-Dicyanamide Complexes: Checking the Rhombicity Effect in Peroxidase Studies. *J. Chem.* **2017**, *2017*, 10 pages. .
(54) Nakamura, T.; Kimura, H.; Okuhara, T.; Yamamura, M.; Nabeshima, T. A Hierarchical Self-Assembly System Built Up from Preorganized Tripodal Helical Metal Complexes. *J. Am. Chem. Soc.* **2016**, *138*, 794−797.
(55) Akine, S.; Taniguchi, T.; Nabeshima, T. Helical metallohost-guest complexes via site-selective transmetalation of homotrinuclear complexes. *J. Am. Chem. Soc.* **2006**, *128*, 15765−15774.
(56) Finelli, A.; Hérault, N.; Crochet, A.; Fromm, K. M. Threading salen-type Cu-and Ni-complexes into one-dimensional coordination

polymers: Solution versus solid state, and the size effect of the alkali metal ion. *Cryst. Growth Des.* **2018**, *18*, 1215−1226.
(57) Akine, S.; Taniguchi, T.; Nabeshima, T. Acyclic bis (N_2O_2 chelate) ligand for trinuclear d-block homo-and heterometal complexes. *Inorg. Chem.* **2008**, *47*, 3255−3264.
(58) Mousavi, M.; Béreau, V.; Costes, J.-P.; Duhayon, C.; Sutter, J.-P. Oligomeric and polymeric organizations of potassium salts with compartmental Schiff-base complexes as ligands. *CrystEngComm* **2011**, *13*, 5908−5914.
(59) Lü, X.; Wong, W.; Wong, W. Self-Assembly of Luminescent Platinum-Salen Schiff-Base Complexes. *Eur. J. Inorg. Chem.* **2008**, *2008*, 523−528.
(60) Cheng, J.; Ma, X.; Zhang, Y.; Liu, J.; Zhou, X.; Xiang, H. Optical chemosensors based on transmetalation of salen-based Schiff base complexes. *Inorg. Chem.* **2014**, *53*, 3210−3219.
(61) Shoora, S. K.; Jain, A. K.; Gupta, V. K. A simple Schiff base based novel optical probe for aluminium (III) ions. *Sens. Actuators, B* **2015**, *216*, 86−104.
(62) Cozzi, P. G. Metal−Salen Schiff base complexes in catalysis: practical aspects. *Chem. Soc. Rev.* **2004**, *33*, 410−421.
(63) Baleizão, C.; Gigante, B.; Sabater, M. J.; Garcia, H.; Corma, A. On the activity of chiral chromium salen complexes covalently bound to solid silicates for the enantioselective epoxide ring opening. *Appl. Catal., A* **2002**, *228*, 279−288.
(64) Canali, L.; Sherrington, D. C. Utilisation of homogeneous and supported chiral metal (salen) complexes in asymmetric catalysis. *Chem. Soc. Rev.* **1999**, *28*, 85−93.
(65) Aluthge, D. C.; Ahn, J. M.; Mehrkhodavandi, P. Overcoming aggregation in indium salen catalysts for isoselective lactide polymerization. *Chem. Sci.* **2015**, *6*, 5284−5292.
(66) Aluthge, D. C.; Patrick, B. O.; Mehrkhodavandi, P. A highly active and site selective indium catalyst for lactide polymerization. *Chem. Commun.* **2013**, *49*, 4295−4297.
(67) Cametti, M.; Nissinen, M.; Dalla Cort, A.; Mandolini, L.; Rissanen, K. Ion Pair Recognition of Quaternary Ammonium and Iminium Salts by Uranyl− Salophen Compounds in Solution and in the Solid State. *J. Am. Chem. Soc.* **2007**, *129*, 3641−3648.
(68) Shellaiah, M.; Wu, Y.-H.; Singh, A.; Raju, M. V. R.; Lin, H.-C. Novel pyrene-and anthracene-based Schiff base derivatives as Cu^{2+} and Fe^{3+} fluorescence turn-on sensors and for aggregation induced emissions. *J. Mater. Chem. A* **2013**, *1*, 1310−1318.
(69) Tyagi, N.; Singh, O.; Singh, U. P.; Ghosh, K. Nitric oxide (NO) reactivity studies on mononuclear iron (II) complexes supported by a tetradentate Schiff base ligand. *RSC Adv.* **2016**, *6*, 115326−115333.
(70) Chiang, L.; Savard, D.; Shimazaki, Y.; Thomas, F.; Storr, T. FeIII Bipyrrolidine Phenoxide Complexes and Their Oxidized Analogues. *Inorg. Chem.* **2014**, *53*, 5810−5819.
(71) Hasan, K.; Fowler, C.; Kwong, P.; Crane, A. K.; Collins, J. L.; Kozak, C. M. Synthesis and structure of iron (III) diamine-bis (phenolate) complexes. *Dalt. Trans.* **2008**, *22*, 2991−2998.
(72) Mayilmurugan, R.; Sankaralingam, M.; Suresh, E.; Palaniandavar, M. Novel square pyramidal iron (III) complexes of linear tetradentate bis (phenolate) ligands as structural and reactive models for intradiol-cleaving 3, 4-PCD enzymes: Quinone formation vs. intradiol cleavage. *Dalt. Trans.* **2010**, *39*, 9611−9625.
(73) Simon, T.; Shellaiah, M.; Srinivasadesikan, V.; Lin, C.-C.; Ko, F.-H.; Sun, K. W.; Lin, M.-C. A simple pyrene based AIEE active schiff base probe for selective naked eye and fluoresence off−on detection of trivalent cations with live cell application. *Sens. Actuators, B* **2016**, *231*, 18−29.
(74) Liu, H.; Yao, L.; Li, B.; Chen, X.; Gao, Y.; Zhang, S.; Li, W.; Lu, P.; Yang, B.; Ma, Y. Excimer-induced high-efficiency fluorescence due to pairwise anthracene stacking in a crystal with long lifetime. *Chem. Commun.* **2016**, *52*, 7356−7359.
(75) Erdemir, S.; Kocyigit, O. Anthracene excimer-based "turn on" fluorescent sensor for Cr^{3+} and Fe^{3+} ions: its application to living cells. *Talanta* **2016**, *158*, 63−69.
(76) Gao, Y.; Liu, H.; Zhang, S.; Gu, Q.; Shen, Y.; Ge, Y.; Yang, B. Excimer formation and evolution of excited state properties in discrete dimeric stacking of an anthracene derivative: a computational investigation. *Phys. Chem. Chem. Phys.* **2018**, *20*, 12129−12137.
(77) Maudoux, N.; Roisnel, T.; Dorcet, V.; Carpentier, J.; Sarazin, Y. Chiral (1, 2)-Diphenylethylene-Salen Complexes of Triel Metals: Coordination Patterns and Mechanistic Considerations in the Isoselective ROP of Lactide. *Chem. - Eur. J.* **2014**, *20*, 6131−6147.
(78) Jones, C.; Junk, P. C.; Black, S. J.; Lewis, J. The molecular structure of [InBr(Salen)($OSMe_2$)]. *Main Group Met. Chem.* **2001**, *24*, 123−124.
(79) Bhattacharya, S.; Mohanta, S. Heterometallic copper (II)−lead (II), nickel (II)−lead (II) and copper (II)−indium (III) compounds derived from an acyclic double-compartment Schiff base ligand. *Inorg. Chim. Acta* **2015**, *432*, 169−175.
(80) Mei, Y.; Borger, J. E.; Wu, D.-J.; Grützmacher, H. Salen supported Al−O−C≡P and Ga−P≡C≡O complexes. *Dalt. Trans.* **2019**, *48*, 4370−4374.
(81) Liao, S.; Yang, X.; Jones, R. A. Self-assembly of luminescent hexanuclear lanthanide salen complexes. *Cryst. Growth Des.* **2012**, *12*, 970−974.
(82) Du, J.; Wang, X.; Zou, X.; Li, Y.; Li, W.; Yao, X.; Li, G. Structures and luminescent sensors of mixed-counterions based salen-type lanthanide coordination polymers. *Luminescence* **2018**, *33*, 1040−1047.
(83) Ren, M.; Xu, Z.-L.; Bao, S.-S.; Wang, T.-T.; Zheng, Z.-H.; Ferreira, R. A. S.; Zheng, L.-M.; Carlos, L. D. Lanthanide salen-type complexes exhibiting single ion magnet and photoluminescent properties. *Dalt. Trans.* **2016**, *45*, 2974−2982.
(84) Li, Q.; Yan, P.; Chen, P.; Hou, G.; Li, G. Salen type sandwich triple-decker tri-and di-nuclear lanthanide complexes. *J. Inorg. Organomet. Polym. Mater.* **2012**, *22*, 1174−1181.
(85) Yang, Y.; Yan, P.-F.; Gao, P.; Gao, T.; Hou, G.-F.; Li, G.-M. Salen-type lanthanide complexes with luminescence and near-infrared (NIR) properties. *J. Inorg. Organomet. Polym. Mater.* **2013**, *23*, 1211−1218.
(86) Rurack, K. Flipping the light switch 'ON'−the design of sensor molecules that show cation-induced fluorescence enhancement with heavy and transition metal ions. *Spectrochim. Acta, Part A* **2001**, *57*, 2161−2195.
(87) Datta, A.; Das, K.; Massera, C.; Clegg, J. K.; Sinha, C.; Huang, J.-H.; Garribba, E. A mixed valent heterometallic Cu(II)/Na(I) coordination polymer with sodium−phenyl bonds. *Dalt. Trans.* **2014**, *43*, 5558−5563.
(88) He, W.; Liu, Z. A fluorescent sensor for Cu^{2+} and Fe^{3+} based on multiple mechanisms. *RSC Adv.* **2016**, *6*, 59073−59080.
(89) Puangsamlee, T.; Tachapermpon, Y.; Kammalun, P.; Sukrat, K.; Wainiphithapong, C.; Sirirak, J.; Wanichacheva, N. Solvent control bifunctional fluorescence probe for selective detection of Cu^{2+} and Hg^{2+} via the excimer of pyrenylacetamide subunits. *J. Lumin.* **2018**, *196*, 227−235.
(90) Choi, Y.-G.; Kwak, G. Solvatochromic fluorescence in an immiscible two-phase system of alcohols and hydrophobic polymers: Distinction between light alcohol and water. *Polymer* **2018**, *141*, 194−201.
(91) Nagata, Y.; Nishikawa, T.; Suginome, M. Solvent-dependent fluorescence and circular dichroism properties of poly(quinoxaline-2, 3-diyl)s bearing pyrene pendants. *Chem. Commun.* **2012**, *48*, 11193−11195.
(92) Liu, W.; Thorp, H. H. Bond valence sum analysis of metal-ligand bond lengths in metalloenzymes and model complexes. 2. Refined distances and other enzymes. *Inorg. Chem.* **1993**, *32*, 4102−4105.